Study of NaF–AlF 3 melts by coupling molecular dynamics, density functional theory, and NMR measurements

Kelly Machado, Didier Zanghi, Vincent Sarou-Kanian, Sylvian Cadars, Mario Burbano, Mathieu Salanne, Catherine Bessada

THE JOURNAL OF PHYSICAL CHEMISTRY C

Article

pubs.acs.org/JPCC

Study of NaF−AlF_3 Melts by Coupling Molecular Dynamics, Density Functional Theory, and NMR Measurements

Kelly Machado,[*,†] Didier Zanghi,[†] Vincent Sarou-Kanian,[†] Sylvian Cadars,[‡] Mario Burbano,[§,∥] Mathieu Salanne,[§] and Catherine Bessada[†]

[†]CEMHTI UPR3079 CNRS, Université Orléans, F-45071 Orléans, France

[‡]Institut des Matériaux Jean Rouxel, B.P. 32229, Université Nantes, CNRS, F-44322 Nantes, France

[§]Sorbonne Université, UPMC Université, Paris 06, CNRS, Laboratoire PHENIX, F-75005 Paris, France

[∥]Maison de la Simulation, USR 3441, CEA, CNRS, INRIA, Université Paris-Sud, Université Versailles, F-91191 Gif-sur-Yvette, France

Supporting Information

ABSTRACT: Improvement of the industrial electrolytic process for aluminum production necessitates a thorough understanding of the underlying ionic structure of the electrolyte, which mainly comprises NaF and AlF_3 at around 965 °C. The chemical and physical properties of this melt strongly depend on the aluminum speciation, which requires a multipronged approach in order to clarify its properties. Here we parametrize a new polarizable ion model (PIM) interatomic potential for the molten NaF−AlF_3 system, which is used to study the liquid properties up to 50 mol % of AlF_3 at high temperatures. The potential parameters are obtained by force fitting to density functional theory (DFT) reference data. Molecular dynamics (MD) simulations are combined with further DFT calculations to determine NMR chemical shifts for ^{27}Al, ^{23}Na, and ^{19}F. An excellent agreement is obtained with experimental values. This enables the study of the dynamic properties of the melts such as viscosity, electrical conductivity, and self-diffusion coefficient.

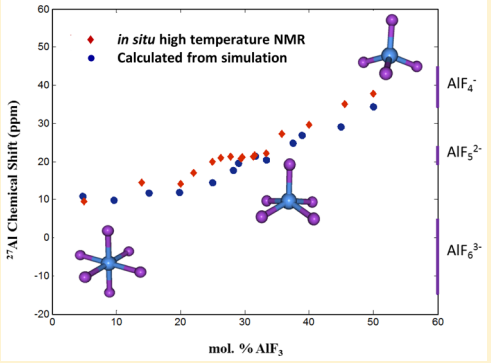

INTRODUCTION

Molten fluorides are investigated for their importance in many metallurgical processes[1−3] such as the Hall−Héroult process for aluminum smelting.[4−7] In the industrial process the alumina (Al_2O_3) is dissolved in a mixture of NaF, AlF_3, and some additives at an operating temperature around 965 °C.[4] Under such high-temperature conditions, these liquids are corrosive and air sensitive, making the experimental approaches difficult. As a consequence, the knowledge of their physical properties, such as viscosity, electrical conductivity, and the speciation, is limited. The results obtained by different techniques may even be in disagreement with each other.[4] Different studies were carried out in order to obtain the structure of NaF−AlF_3 mixtures at high temperature. Raman[8,9] and NMR[5,7] spectroscopies have succeeded in identifying and in quantifying the anions present in the system, i.e., free F^-, as well as different aluminum-bearing fluorinated species, AlF_6^{3-}, AlF_5^{2-}, and AlF_4^-. However, the exact concentration of AlF_5^{2-} anions remains a controversial issue. For example, Dewing concluded from his thermodynamic models based on activity data that AlF_5^{2-} should be a major entity,[10] in contradiction with the model of Solheim and Sterten.[11] The existence of free fluoride ions in cryolite melts has also been challenged by Khramov and Shurov[12] with a formal stoichiometric study. Finally, the existence of bridged complexes in these melts (i.e., the presence of Al−F−Al bonds) has been examined from some authors. Yet it is difficult to make explicit predictions on the structure of dimers in cryolitic melts. Both thermodynamic models from Dewing[10] and from Solheim and Sterten[11] predicted the existence of the complex $Al_2F_7^-$.

Nowadays molecular dynamics (MD) simulations are a complementary approach for understanding the chemistry of molten salts. Liska et al.[13] used the Born−Mayer type pair potential functions (PPFs) to study molten cryolite (Na_3AlF_6) and concluded that the average coordination number of aluminum is AlF_6^-. However, these results do not agree with experimental data that have shown that 6-fold coordinated aluminum is present at low percentage only. Further MD simulations using a polarizable ionic potential were performed for the cryolite (Na_3AlF_6), chiolite ($Na_5Al_3F_{14}$), and $NaAlF_4$ compositions within the NaF−AlF_3 binary system,[14−16] in which the speciation and the lifetime of fluoroaluminate species were calculated. The 5-fold coordinated AlF_5^{2-} ion was concluded to be the main species in cryolite. The Raman spectra were also calculated from the latter work, providing a general good agreement with only a few differences between the experimental and the calculated vibrational frequencies: The absolute positions of the calculated Raman bands are about

Received: February 16, 2017
Revised: April 28, 2017
Published: May 2, 2017

DOI: 10.1021/acs.jpcc.7b01530
J. Phys. Chem. C 2017, 121, 10289−10297

100 cm^{-1} higher, but the trend from Na_3AlF_6 to $NaAlF_4$ is nevertheless well reproduced. The observed differences were attributed to the fact that the interaction potential had been derived for the crystalline state, while the comparison was made in the liquid state. Polarizable ion models were also used to simulate the ionic motion in crystalline cryolite,[17] the ionic structure of the molten $LiF-ZrF_4$ system,[18] as well as the thermal conductivity of molten cryolite.[19] More recently, a DFT-based MD study was aimed at simulating cryolite in various states, ranging from the low-temperature solid (α) to the high-temperature solid phase (β) and to the molten state.[20] In the liquid, coordination numbers of 4, 5, and 6 were observed. The authors also observed the formation of fluoride-bridged complexes with compositions $Al_2F_8^{2-}$ (6%), $Al_2F_9^{3-}$ (50%), $Al_2F_{10}^{4-}$ (37%), and $Al_2F_{11}^{5-}$ (7%).

Despite these various studies, we lack a precise knowledge of the nature of the complexes, their lifetime, and their evolution with the melt composition and the temperature. In particular, quantitative agreement between the experimental and the simulation data remains to be achieved. To this end, we introduce in this work a new polarizable interaction potential for $NaF-AlF_3$ melts. All the parameters involved in the potential are extracted from first-principles density functional theory (DFT) calculations through an extended dipole-matching and force-matching procedure.[21−23] We validate it on a large range of system compositions, by computing the NMR chemical shifts of each nucleus at the DFT level,[24,25] which are performed on configurations generated along the simulations *without further optimization*. The chemical shift is one of the most sensitive markers of the local structure. It is sensitive to the first neighbors, i.e., to the coordination numbers and the corresponding bond length. The calculated parameters are compared with the *in situ* NMR experimental values. A quantitative agreement is obtained, which allows us to describe accurately the structure of the melts. We then interpret the variations of a series of physical properties in light of the presence of the various species and calculate the transport properties of the melt.

METHODS

NMR Experiments. High-temperature NMR measurements were performed on a laser heating NMR setup developed at CEMHTI Orleans (France) using a Bruker AVANCE I NMR spectrometer operating at 9.4 T. The CO_2 lasers (λ = 10.6 μm, 250 W) heat directly the top and the bottom of the container with the sample, allowing them to reach temperatures up to 1500 °C. The experimental setup has been described in detail in previous publications.[26−28] The samples were put in a boron nitride crucible air tightly closed by a screw cap. Crucibles are protected from oxidation during the experiments at high temperature by a continuous argon flow. The spectra were collected for several $NaF-AlF_3$ compositions, ranging from 5 to 50 mol % of AlF_3 where the chemical shifts of all nuclei (^{27}Al, ^{23}Na, ^{19}F) are referenced to 1 M aqueous solutions of $Al(NO_3)_3$, NaCl, and $CFCl_3$, respectively.

In the liquid state, the rapid tumbling of species averages the anisotropic (direction-dependent) shielding components to zero. The chemical shift is therefore only described by the isotropic chemical shift due to the rapid time-averaged molecular motion. This causes a narrow signal, giving rise to the isotropic chemical shifts for each species: $\delta_{iso} = [\sigma_{ref} - \sigma_{iso}]$. The isotropic tensor ($\sigma_{iso}$) representing the screening on the core is equal to the average of the tensor's diagonal elements: $\sigma_{iso} = (\sigma_{xx} + \sigma_{yy} + \sigma_{zz})/3$. Moreover, in molten fluorides, the different species present in the system are in rapid exchange compared to the NMR time scale, which results in a single Lorentzian line instead of several narrow signals from each chemical species. Its position (in ppm) is given by the average over time of the chemical shifts of all configurations sampled by the species during acquisition, weighted by their proportion, such that $\delta = \sum_i X_{A_i}^N \delta^N(A_i)$ where, $X_{A_i}^N$ is the atomic fraction of nuclei N inside the species A_i and $\delta^N(A_i)$ is the corresponding chemical shift.

For each experiment, the samples were heated at temperatures up to 1305 K. In each case, the spectra acquisition started 5 min after reaching the desired temperature to ensure that thermal equilibrium was reached. The NMR signals for ^{19}F, ^{23}Na, and ^{27}Al were then recorded sequentially. The experimental values reported in this work are in good agreement with previous published data obtained by Lacassagne et al.[5] and Nuta et al.,[7] where only the bottom part of the crucible containing the samples was heated by a CO_2 laser (λ = 10.6 μm, 120 W). In the present work a better temperature homogeneity is expected to the dual heating of the sample from the top and the bottom.

High-temperature NMR also provides an accurate measurement of self-diffusion coefficients through the use of pulsed field gradient NMR. An external linear magnetic field gradient is applied along one sample axis, enabling us to track the positions of the studied nuclei. Combined with the laser heating, *in situ* self-diffusion coefficients were measured in the melts up to 1305 K.[26,29]

Polarizable Ion Model. The general form of the interatomic potential used for the study of molten fluorides is derived from the Born model[30] which separates the interactions between the various species into pairwise additive interactions. For each ion pair, the model is composed of four separate elements, $V^{total} = V^{charge} + V^{repulsion} + V^{dispersion} + V^{polarization}$, that represent (i) the Coulombic interactions between the charges (which are the formal valence charges), (ii) the overlap repulsion between the electronic clouds around each ion, (iii) the dispersion component which includes dipole−dipole and dipole−quadrupole dispersion terms, and (iv) the dipole polarization effects. The polarization contribution is specific to this model. It represents the response of the electronic cloud of a given ion to the local electric field due to the other ions. This polarization effect plays an important role in the formation of highly coordinated multivalent ions in molten fluorides as well as in the dynamic properties such as the diffusion of ionic species.[31] A detailed description of the analytical expressions used in this work is presented in the Supporting Information.

Potential Parametrization. The potential parametrization calculations were performed on nine high-temperature ionic configurations to cover a wide range of compositions going from 5 to 50 mol % of AlF_3. The use of several configurations during the potential parametrization allows a better and importantly more robust description of the binary system. For each of them, reference DFT calculations were made in order to obtain the forces and dipoles of each atom and the stress tensor of the cell. Each simulation cell contained approximately 200 ions. The DFT calculations were carried out by using a generalized gradient approximation (GGA) with a Perdew, Burke, and Ernzerhof (PBE) exchange-correlation functional[32] as implemented in the Vienna ab-initio simulation package (VASP).[33−36] In previous works, the dispersion

DOI: 10.1021/acs.jpcc.7b01530
J. Phys. Chem. C 2017, 121, 10289−10297

parameters were not included in the fitting procedure, but they were fixed to some given values. The novelty is that, in the present study, dispersion interactions are explicitly calculated through the use of the DFT-D3 correction[37] which gives a better representation of the interaction. The plane-wave cutoff energy (E_{cut}) was fixed to 800 eV after several tests on the convergence of the total energy of the system. For fluorine, a core radius of 1.52 Å was used with 2s and 2p valence orbitals, and for aluminum the core radius was 1.9 Å with 3s and 3p of valence orbitals, and for sodium 1.5 Å with 2s, 2p, and 3s. The dipoles were extracted using the maximally localized Wannier function (MLWF) formalism.[38−40] As to the forces acting on each ion and the stress tensors, they are determined directly from each DFT calculation using the Hellmann−Feynman theorem.

Then the polarizable ion model (PIM) is parametrized by simultaneously minimizing the following objective function using a nongradient simplex and MIGRAD method[41] as implemented in the package MINUIT: $\chi^2 = \varphi\chi^2_{\text{Forces}} + \delta\chi^2_{\text{Dipoles}} + \gamma\chi^2_{\text{Stress}}$, where φ, δ, and γ are the weight of each component, and in our study, $\varphi = \delta = 1$ and $\gamma = 0.1$. In practice, this is done by minimizing the following eqs 1−3

$$\chi^2_{\text{Forces}} = \frac{1}{N_c}\sum_{j=1}^{N_c}\frac{1}{N_j}\sum_{i=1}^{N_j}\frac{|F^i_{\text{DFT}} - F^i_{\text{classical}}|^2}{|F^i_{\text{DFT}}|^2} \quad (1)$$

$$\chi^2_{\text{Dipoles}} = \frac{1}{N_c}\sum_{j=1}^{N_c}\frac{1}{N_j}\sum_{i=1}^{N_j}\frac{|\mu^i_{\text{DFT}} - \mu^i_{\text{classical}}|^2}{|\mu^i_{\text{DFT}}|^2} \quad (2)$$

$$\chi^2_{\text{Stress}} = \frac{1}{N_c}\sum_{j=1}^{N_c}\frac{\sum_{\alpha\beta}|\sigma^i_{\alpha\beta,\text{DFT}} - \sigma^i_{\alpha\beta,\text{classical}}|^2}{\sum_{\alpha\beta}|\sigma^i_{\alpha\beta,\text{DFT}}|^2} \quad (3)$$

where N_c is the number of configurations, N_j the number of ions in configuration j, F^i the force of ion i, $\sigma^i_{\alpha\beta}$ the stress tensor, and μ^i the dipole.

Figure 1 provides a visual representation of the matching between the x-component of the forces (top panel) and dipoles

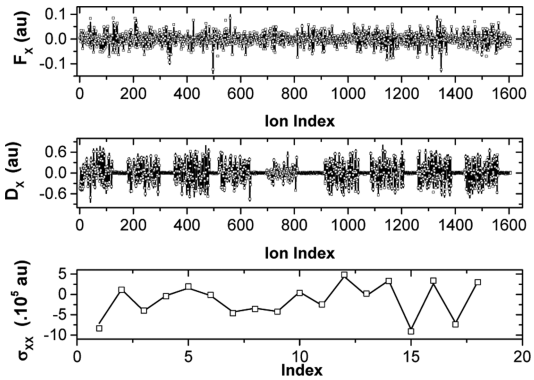

Figure 1. x-component of the forces and dipoles and xx-component of the stress tensor obtained by DFT calculations (line) and with the fitted PIM potential (□) for a set of nine ionic configurations (values are in atomic units).

(medium panel) and the xx-component of the stress tensor (bottom panel) obtained from DFT (line) and PIM (square). The nine configurations used to parametrize the potential are shown, which corresponds to 1812 forces and 1606 induced dipole components (the Al ions being nonpolarizable) for each axis (x, y, and z) and 9 sets of stress with 6 components each (xx, xy, xz, yy, yz, and zz). The resulting parameters are reported in Table 1.

Table 1. Pair Potential Parameters (All of the Parameters Are Given in Atomic Units (au))[a]

ion pair	B_{ij}	α_{ij}	C^6_{ij}	C^8_{ij}
F^- - F^-	392.57	2.48	3.11	104.93
F^- - Al^{3+}	37.97	1.88	1.89	100.43
F^- - Na^+	52.4	1.97	9.43	132.55
Al^{3+} - Al^{3+}	7.57	6.50	60.0	400.00
Al^{3+} - Na^+	0.23	6.37	29.98	400.00
Na^+ - Na^+	0.37	1.38	3.79	399.88

[a]The dipole polarizabilities of fluoride and sodium ions were set to 8.158 au and 0.887 au, respectively. For aluminum the polarizability was set to zero.

Molecular Dynamics Simulations. The classical MD simulations are performed with the PIM code.[42−44] In a first step, the isothermal−isobaric (NPT) canonical ensemble was used. The temperature and the average internal pressure are held at 1305 K and 0 GPa, respectively, by coupling the simulation cell (which has cubic shape) to Nosé−Hoover thermostat chains and a barostat.[45,46] The relaxation time that sets the strength of the coupling of the system to the thermostats or to the barostat was fixed to 20 ps. The aim of this equilibration period, whose duration is typically 100 ps, is to allow the system to reach equilibrium prior to data collection. The time step for integrating the equations of motion was fixed to 1 fs.

The production phase is carried out in the canonical ensemble (NVT). The parameters of the cubic cells (compositions, number of atoms, and volumes) used for simulations are provided in Table 2. The cell length is fixed to

Table 2. Molecular Dynamics Simulations Conditions

no.	mol % AlF_3	N_{F^-}	N_{Na^+}	$N_{Al^{3+}}$	volume (Å^3)
1	5	115	100	5	3426
2	10	124	94	10	3450
3	15	138	90	16	3405
4	20	148	85	21	3536
5	25	120	60	20	3543
6	28	122	56	22	3609
7	29	120	54	22	3726
8	31	124	52	24	4182
9	33	125	50	25	4025
10	37	126	45	27	2989
11	39	128	44	28	3954
12	45	131	38	31	4035
13	50	132	33	33	4215

the stable average value of the NPT run, and an example of the variation of the density with time is shown in Figure 2, for the configuration of 67 mol % NaF−33 mol % AlF_3 at 1305 K. At equilibrium, the density is 1.97 ± 0.08 g/cm^3, which corresponds to a cell length of 15.25 Å. The production simulations were run from 1 to 5 ns, i.e., for a sufficiently long time to allow the convergence of the transport properties (viscosity, self-diffusion, and ionic conductivity...).

NMR DFT Computational Details. The isotropic chemical shifts δ_{iso} of the three nuclei (^{19}F, ^{27}Al, ^{23}Na) in the molten

DOI: 10.1021/acs.jpcc.7b01530
J. Phys. Chem. C 2017, 121, 10289−10297

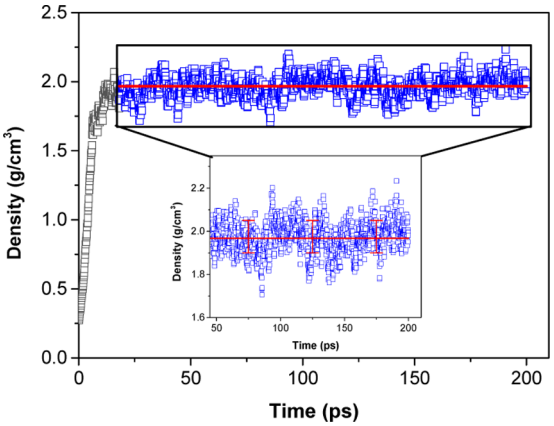

Figure 2. Variation of the density during the NPT simulation for the [67−33 mol %] of NaF−AlF_3 composition at 1305 K. The red line is the averaged density with its standard deviation.

NaF−AlF_3 system have been conducted with the NMR-CASTEP code[24,25] which is based on the density functional theory (DFT) plane-wave pseudopotential framework to compute the isotropic shielding tensor σ_{iso} representing the screening that receives the core. By convention, the isotropic chemical shifts are related to the shielding by a reference shielding σ_{ref} from a crystalline compound known, according to the following relationship: $\delta_{iso} = \sigma_{ref} - \sigma_{iso}$.

Calculations of the chemical shifts are particularly sensitive to dynamics as the shifts are nonlinear and anharmonic effects are significant. Since the measurement time of an NMR experiment takes a few milliseconds, it is therefore essential to account for the motion in the calculations especially in the case of liquids. To overcome this problem, the dynamics has been accounted for by averaging over an ensemble of configurations generated by classical MD at a given temperature to track the ionic trajectories on long time scales and relatively large systems.[47] The computations of NMR parameters were performed on evenly spaced snapshots extracted from the MD simulations in the NVT ensemble without further optimization. In the following, we sample configurations every 100 ps. This spacing ensures that the configurations are uncorrelated.[48] To limit the NMR computation time, we chose to work with small cubic cells containing approximately 200 atoms rather than on large systems while increasing the number of extracted snapshots (10−15 according to the studied system), a procedure which assumes that the system is ergodic. For each snapshot, the individual chemical shielding tensor is calculated for all the nuclei of the system. The isotropic shielding values are then averaged to give a mean value for each atomic configuration. This value is averaged afterward with the other values calculated for all the configurations to find the mean value and its standard deviation.

The calculations of chemical shielding tensors have been done using the gauge including projector-augmented wave[49] (GIPAW) method implemented in CASTEP. The PBE functional[32] was again used for the exchange-correlation energy, and the core−valence interactions were described by ultrasoft pseudopotentials (USPPs).[50] The USPPs were generated during "the on the fly" generator (OTFG_USPP) included in CASTEP that allows us to choose some parameters which govern the pseudopotential generation (Table 3) and instead to choose a file from the CASTEP database.

Table 3. Pseudopotential Parameters for NMR Calculations

atom	core radius (Å)	valence orbitals	number of electrons
fluoride	0.74	2s and 2p	7
aluminum	1.06	3s and 3p	3
sodium	0.69	2s, 2p, and 3s	9

The wave functions were expanded on a plane-wave basis set with a cutoff energy of 610 eV defined after completing convergence tests on the energy of the system (note that the cutoff used for the force fitting was larger to ensure convergence of the forces and of the stress tensor, which is not necessary here). The Brillouin zone was sampled using a Monkhorst−Pack grid[51] spacing of 0.05 $Å^{-1}$ corresponding to a k-point mesh of 1 × 1 × 1. This grid is sufficient to obtain converged isotropic chemical shielding within 1 ppm or less.

In order to assign the NMR resonances from GIPAW computations, the definition of calibration curve relating isotropic chemical shift and shielding is necessary. In practice for a type of given nucleus, the link between the calculated δ_{iso} and the computed σ_{iso} is obtained by a linear regression between measured isotropic chemical shifts and calculated isotropic chemical shielding for a series of solid compounds by keeping the same pseudopotentials and functional. These references have been chosen to cover a large domain of chemical shifts for each type of nuclei, which, provided the electronic structure is correct, ensure that computed chemical shifts can be directly compared to experimental values. In the case of ^{19}F, we used the relationship reported by Sadoc et al.[52] As for ^{27}Al and ^{23}Na this relationship was established in our laboratory, resulting in the following: $\delta_{iso} = -1.076\sigma_{iso} + 590.8$ and $\delta_{iso} = -0.840\ \sigma_{iso} + 467.9$ for ^{27}Al and ^{23}Na, respectively.

RESULTS AND DISCUSSION

The quality of the interaction potential used for MD simulation of the NaF−AlF_3 system can be assessed by comparing the simulated physical quantities to experimental data. In the following section, we provide quantitative comparisons of the density, the chemical shift, the conductivity, the viscosity, and self-diffusion coefficients. The variations of these properties with composition are rationalized from the speciation of the melts.

Density. The calculated and experimental[53] densities are in good agreement at 1305 K for the whole range of NaF−AlF_3 compositions, as demonstrated in Figure 3. This ensures that the simulations are performed at the correct thermodynamic state. It is worth noting that the density undergoes nontrivial variations, with a maximum occurring at the cryolite composition, which is probably due to structural changes in the melt.

Chemical Shifts. The calculated chemical shifts for the three nuclei at the NaF−AlF_3 [85−15 mol %] composition and 1305 K are reported in Figure 4. The converged values of the calculated chemical shift are $\delta^{19}F = (-206.8 \pm 0.8)$ ppm, $\delta^{23}Na = (-1.9 \pm 0.9)$ ppm, and $\delta^{27}Al = (11.7 \pm 2.1)$ ppm. More significant variation is found for ^{27}Al, and this is directly related to the small number of Al atoms in every snapshot.

The influence of the number of snapshots extracted for NMR calculation was tested, for two different compositions (50 mol % and 25 mol % of AlF_3). Only a small difference was observed (±0.5 ppm for ^{27}Al, ±0.6 ppm for ^{19}F, and ±0.2 ppm for ^{23}Na) when using either 12 or 22 snapshots. These results prove that beyond 10 snapshots the averaged chemical shift converges for

DOI: 10.1021/acs.jpcc.7b01530
J. Phys. Chem. C 2017, 121, 10289−10297

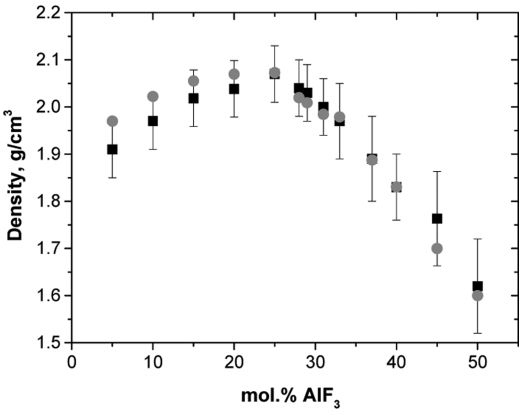

Figure 3. Evolution of calculated (black filled square) and experimental[53] (gray filled circle) density as a function of mol % AlF_3 at 1305 K.

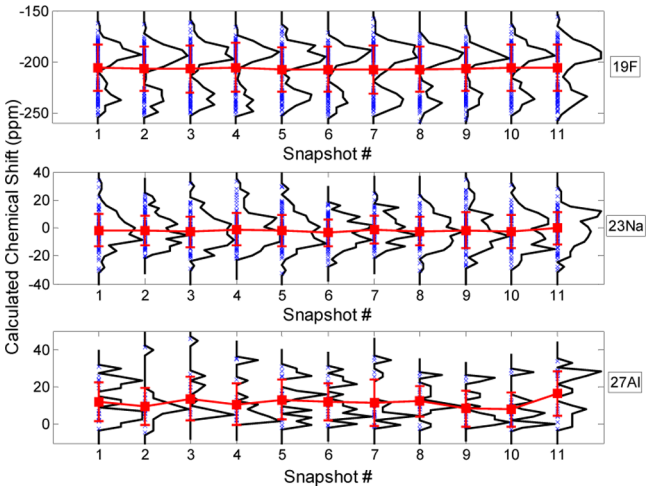

Figure 4. Variation of chemical shift calculation between snapshots for the $NaF-AlF_3$ [85−15 mol %] composition at 1305 K. Blue x symbols: The chemical shift for each individual nucleus of the snapshot. Black line: distribution of the chemical shift of the three studied nuclei (^{19}F, ^{27}Al, and ^{23}Na) for each snapshot. Red filled square symbols: average of the isotropic chemical shift and its standard deviation for each snapshot.

such systems. The NMR parameter calculations give access to information that is not available experimentally, due to the rapid exchange of the different species at high temperature, such as the "static" distributions of instantaneous chemical shifts, shown as a black solid line in Figure 4. For instance, the ^{19}F distribution calculated for the composition with 15 mol % AlF_3 (Figure 4) shows two very distinct contributions: one centered at ca. −230 ppm which may be assigned to free F^- ions and another one at ca. −190 ppm assigned to F atoms bonded to (at least one) Al atom. This separation indicates that, even in the high-temperature melt, the instantaneous local electronic structures around these two types of F atoms are profoundly different. Furthermore, the ^{27}Al distribution, when sufficiently smoothed by averaging over an appropriate number of snapshots, reveals a separation between the (albeit partially overlapping) contributions from six-, five-, and (in other compositions, not shown) four-coordinated Al atoms, centered at −5 ± 10 ppm, 22 ± 2 ppm, and 40 ± 5 ppm, respectively.

The chemical shifts computed using the coupled MD/DFT approach are compared with experimental data on Figure 5.

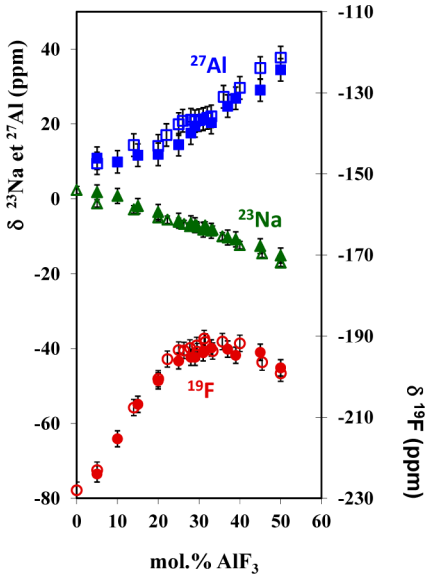

Figure 5. Comparison between the calculated (full markers) and experimental (empty markers)[5−7] chemical shifts depending on the molar fraction of AlF_3 at 1305 K.

The uncertainty of the calculated chemical shift was estimated to be ±3 ppm for ^{27}Al and ±2 ppm for ^{19}F and ^{23}Na; it is comparable with the uncertainty in NMR experimental measurements: 2 ppm for ^{19}F, ±3 ppm for ^{27}Al, and ±1 ppm for ^{23}Na. A good agreement between the calculated and experimental shift values is observed, which indicates that the polarizable ion model used in these simulations is able to reproduce accurately the local structure around each nucleus in the $NaF-AlF_3$ molten salt.

The variation of the ^{23}Na and ^{27}Al chemical shifts with the AlF_3 concentration is monotonous, which shows that the changes of their local environment follow a simple trend. This contrasts with ^{19}F, for which the chemical shift shows a maximum. At 0 mol % of AlF_3 the free fluoride is the single anionic species with a ^{19}F chemical shift around −230 ppm, and as AlF_3 is added the fluorine chemical shift increases because of the decrease of free fluoride contribution. A plateau is then reached in the region corresponding to concentrations of 25−35 mol %, followed by a decrease of the chemical shift. As for the density, this behavior is likely to arise from the formation of particular local environments for the fluoride anions.

Coordination Number. In order to interpret the variations of the density and of the ^{19}F chemical shift with composition, we thus analyze various structural quantities. First the radial distribution functions (RDFs), noted $g(r)$, provide information about the local ionic arrangement around a selected atom. Selected partial RDFs for 31 mol % AlF_3 are given in Figure 6. The Al−F RDF has a first peak that is very intense and narrow, which is characteristic of a strong covalent interaction leading to the formation of well-defined coordination complexes (AlF_x^{3-x}). In addition, it shows a well-defined minimum with a very low value of $g(r)$. This indicates that the F^- ions have to cross a large barrier to exit from the first sphere of solvation of the aluminum ions.[54] In contrast, the first peak of the Na−F RDF is much less intense and wider, revealing a loosely bound first coordination sphere of anions around the Na^+ cations. The corresponding first neighbor distances are 1.54 Å for the pair Al−F and 1.77 Å for Na−F.

DOI: 10.1021/acs.jpcc.7b01530
J. Phys. Chem. C 2017, 121, 10289−10297

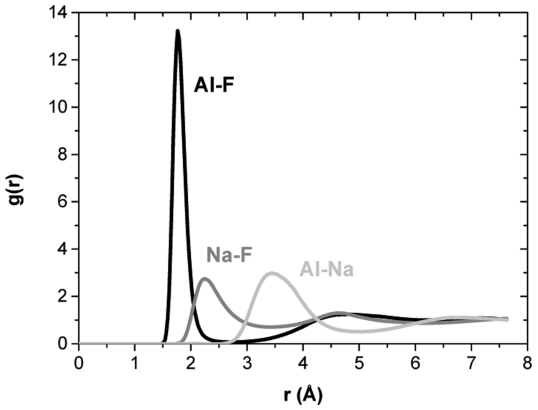

Figure 6. Partial pair radial distribution functions obtained by MD for [69−31 mol %] of $NaF-AlF_3$ at 1305 K.

As shown in Table 4, the position of the Al−F RDF first maximum decreases with the amount of AlF_3, from 1.80 Å for 25 mol % AlF_3 to 1.74 Å for 40 mol % AlF_3 indicating a decrease of the Al−F bond length. The coordination numbers are obtained using the first minimum of the RDF as the radius of the shell to count the number of anions around a given cation. Furthermore, as already described in previous works,[5,7] it is also possible to extract the anionic fractions of these melts from the evolution of the ^{19}F and ^{27}Al experimental chemical shifts, using eqs 4 and 5 with the chemical shift of each species (AlF_x^{3-x} and F^-).

Table 4. RDF Analysis for Al−F Pairs at Different Compositions at 1305 K

AlF_3 (mol %)	position of the first maximum (Å)	position of the first minimum (Å)
40	1.74	2.18
33	1.77	2.22
25	1.80	2.26

$$\delta_F = X^F_F \cdot \delta^F_{F^-} + X^F_{AlF_6^{3-}} \cdot \delta^F_{AlF_6^{3-}} + X^F_{AlF_5^{2-}} \cdot \delta^F_{AlF_5^{2-}} + X^F_{AlF_4^-} \delta^F_{AlF_4^-} \quad (4)$$

$$\delta_{Al} = X^{Al}_{AlF_6^{3-}} \cdot \delta^{Al}_{AlF_6^{3-}} + X^{Al}_{AlF_5^{2-}} \cdot \delta^{Al}_{AlF_5^{2-}} + X^{Al}_{AlF_4^-} \delta^{Al}_{AlF_4^-}$$

The average coordination numbers around aluminum obtained from calculations and NMR experiments are plotted in Figure 7. A very good agreement is observed, with a decrease of the Al coordination from 6 to 4 when the concentration of AlF_3 increases.

In Figure 8 the proportion of each species, as extracted from the MD calculations, is compared with NMR experimental data. Apart from a deviation of 10−15% between the two approaches for 6-fold coordinated aluminum, a good agreement is noted for the different species along the whole range of AlF_3 compositions. It appears that AlF_4^- entities start to form at 25 mol %, and it rapidly becomes the dominant fluoroaluminate species. This species has a similar radius as the 5-fold and 6-fold coordinated ones but a lower mass. We can therefore deduce that its formation is at the origin of the variation of the density shown on Figure 3.

However, concerning the chemical shift, it would be necessary to analyze the local structure around fluoride ions. Indeed, they can either be free, singly bonded to an aluminum ion, or bridging between two complexes when they participate

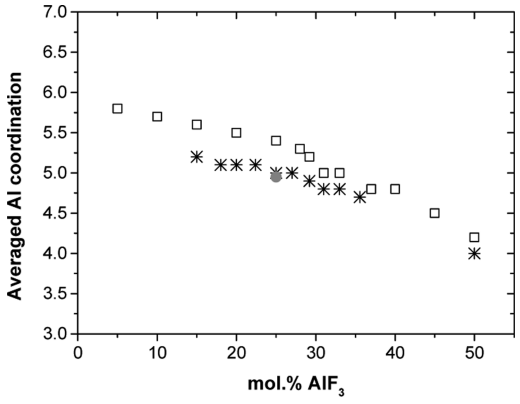

Figure 7. Average aluminum coordination numbers from NMR experiments (∗), MD calculations (□), and DFT-based MD simulation from Bucko and Simko[20] (●).

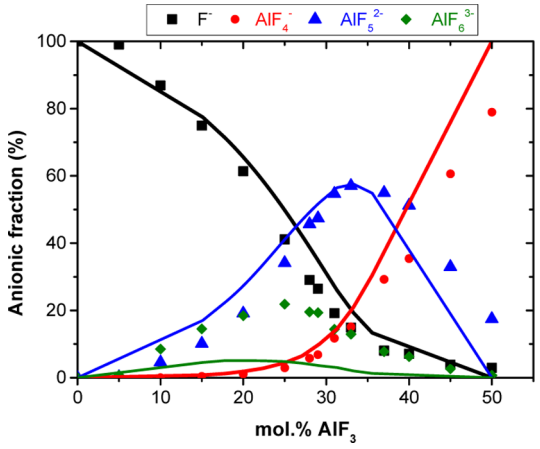

Figure 8. Anionic fractions extracted from NMR experiment (lines) at 1273 K and MD simulations (markers) at 1305 K.

to two bonds (which correspond to $Al_2F_m^{6-m}$ entities). The corresponding fractions are provided on Figure 9. Bridging fluorides appear for a concentration of AlF_3 larger than 25 mol %, with a corresponding fluoride fraction going up to 10%. It is therefore clear that their formation is favored by the presence of 4-fold coordinated aluminum ions. On Figure 9, we also reproduce the variation of the ^{19}F chemical shift. Its decrease

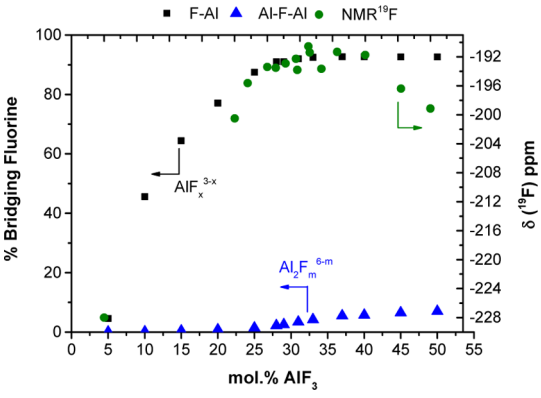

Figure 9. Percentage of one-fold F−Al (black solid square) and 2-fold Al−F−Al (blue solid triange) coordinated fluoride ions compared with the NMR chemical shift of ^{19}F (green solid circle) for varying concentrations of AlF_3, for a temperature of 1305 K.

DOI: 10.1021/acs.jpcc.7b01530
J. Phys. Chem. C 2017, 121, 10289−10297

for concentrations larger than 35 mol % is correlated with the formation of bridging fluorides.

Transport Properties. Electrical conductivity is a very important property for industrial applications of molten salts. In MD simulations, it is calculated by taking into account the correlations of the displacements between the different species, according to the formula

$$\sigma = \frac{e^2}{k_B TV} \lim_{t\to\infty} \frac{1}{6t} (|\sum_i q_i \delta r_i(t)|^2) \quad (6)$$

where e is the elementary charge; q_i is the formal charge of the atom i; and $\delta_{ri}(t)$ is the displacement of ion i in time t. The calculated electrical conductivities are compared with the experimental impedance measurements based on the work of Edwards et al.[53,55] and another study where it was measured by the continuously varying cell constant (CVCC) technique[56] on Figure 10. A good agreement is obtained across the whole composition range: both approaches predict a decrease with the AlF_3 fraction.

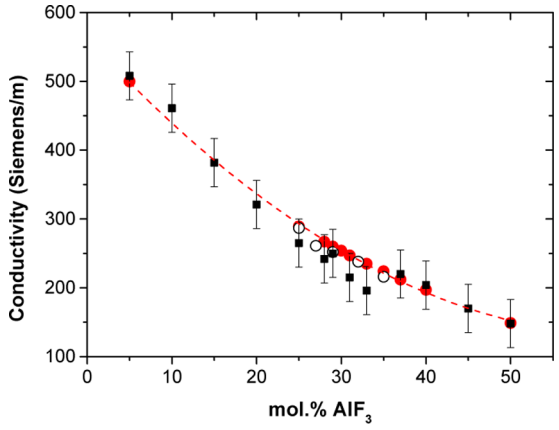

Figure 10. Electrical conductivity of molten NaF−AlF_3 mixtures as a function of the mol % of AlF_3 at 1305 K. Squares are molecular dynamics results; empty circles are experimental data from ref 56; and red circles are experimental data.[53−55]

The viscosity of a system is calculated from the time integral of the autocorrelation function of the anisotropic elements of the stress tensor by the Green−Kubo formula

$$\eta(t) = \frac{1}{k_B TV} \int_0^\infty |\sigma_{\alpha\beta}(0)\sigma_{\alpha\beta}(\tau)| d\tau \quad (7)$$

where $\sigma_{\alpha\beta}$ is one of the five components of the stress tensor. Calculated viscosity for low mol % of AlF_3 is in agreement with the experimental results, and then we obtained higher values, by about a factor of 2, between 25 and 50 mol %, as shown on Figure 11. The difference may be attributed to the relatively small size of the simulation cell.

Finally, self-diffusion coefficients of each species are extracted from MD simulations, from the long-time slope of mean squared displacement

$$D_\alpha = \lim_{t\to\infty} \frac{1}{6t} (|\delta r_i(t)|^2) \quad (8)$$

The correction proposed by Yeh and Hummer[57] was introduced to correct for the effect of periodic boundary conditions. The self-diffusion coefficients of fluoride, sodium, and aluminum ions along the 1305 K isotherm are displayed in

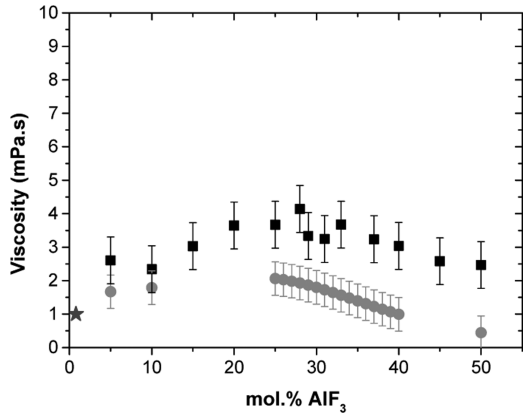

Figure 11. Viscosity of molten NaF−AlF_3 mixtures as a function of AlF_3 mol % at 1305 K. Squares are molecular dynamics results, and circles are experimental data.[53−55] As a guideline, the viscosity of water at 20 °C is shown with a star on the abscissa.

Figure 12. The measure of self-diffusion coefficients was obtained earlier by Gobet et al. using *in situ* high-temperature

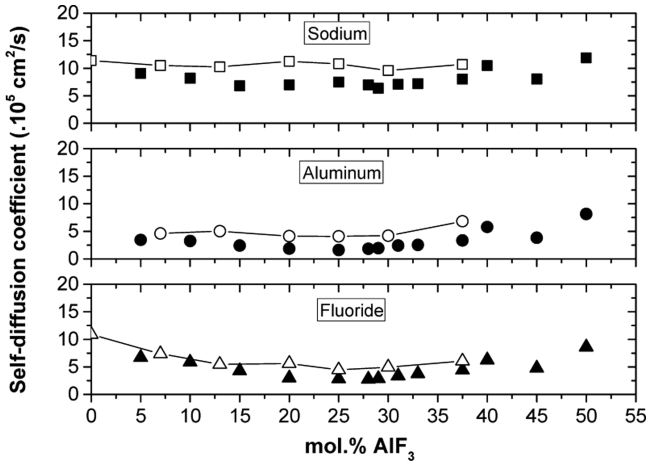

Figure 12. Self-diffusion coefficients of sodium (squares), aluminum (circles), and fluor (triangles) ions in NaF−AlF_3 at 1305 K as a function of the mol % AlF_3. Full symbols indicate molecular dynamics, and open symbols indicate NMR experimental data.[58]

pulsed field gradient NMR combined with laser heating.[58] As sodium ions are free (i.e., they do not participate in stable structural entities), their diffusion coefficients are higher than those of Al and F. In the case of fluoride ions we can see that the value decreases with the amount of AlF_3 and tends to converge toward one of the aluminum ions. This is consistent with the structural analysis, which showed a decrease of the proportion of free fluoride in the melt and an increase of the involvement of fluoride in AlF_x^{3-x} complexes. No particular variation of the diffusion of the species is observed upon the formation of bridging fluorides, but their relative concentration may be too small to yield a visible impact.

CONCLUSION

The aim of this work was to build an interatomic potential able to describe the NaF−AlF_3 system at high temperature. For this purpose, we applied the method proposed by Madden et al., which is based on DFT calculations: no experimental results are used for the potential parametrization. Parametrization results

DOI: 10.1021/acs.jpcc.7b01530
J. Phys. Chem. C 2017, 121, 10289−10297

from a fit between forces and dipoles of each atoms and stress of each configuration calculated by DFT and molecular dynamics. The *ab initio* derived polarizable interaction potential reproduces well the structure of the molten mixtures of the binary NaF−AlF_3 at 1305 K in a wide range of compositions (0−50 mol %). The dynamic properties, such as the self-diffusion coefficients and the electrical conductivity, were also computed and compared with experimental results. The anionic structure was calculated for the first time for a wide range of compositions of NaF−AlF_3 in agreement with experimental results. To our knowledge this is the first time that a model capable of reproducing the physicochemical behavior of the NaF−AlF_3 over such a broad composition range and with this level of accuracy is reported. Future work will be devoted to the inclusion of alumina Al_2O_3 in such melts, in order to understand how the presence of oxide ions impacts the structure and the physical properties of the melts.

■ ASSOCIATED CONTENT

Supporting Information

The Supporting Information is available free of charge on the ACS Publications website at DOI: 10.1021/acs.jpcc.7b01530.

Supporting equations of the dispersion component, repulsive overlap interaction, and polarization effect between two ions (PDF)

■ AUTHOR INFORMATION

Corresponding Author

*E-mail: kelly.machado@cnrs-orleans.fr.

ORCID

Kelly Machado: 0000-0001-6045-5734

Mathieu Salanne: 0000-0002-1753-491X

Notes

The authors declare no competing financial interest.

■ ACKNOWLEDGMENTS

This study was financially supported by the ANR MIMINELA project of the French National Research Agency. All computations presented in this work have been performed at the "Centre de Calcul Scientifique en Région Centre" facility (CCRS − Orléans, France) under the CASCIMODOT program. We thank Vincent Stabrowski from Rio Tinto Aluminum (Voreppe, France) for all discussions.

■ REFERENCES

(1) Chen, G. Z.; Fray, D. J.; Farthing, T. W. Direct Electrochemical Reduction of Titanium Dioxide to Titanium in Molten Calcium Chloride. *Nature* **2000**, *407*, 361−364.

(2) Ghallali, H. El; Groult, H.; Barhoun, A.; Draoui, K.; Krulic, D.; Lantelme, F. Electrochemical Synthesis of Ni−Sn Alloys in Molten LiCl−KCl. *Electrochim. Acta* **2009**, *54*, 3152−3160.

(3) Groult, H.; Barhoun, A.; Briot, E.; Lantelme, F.; Julien, C. M. Electrodeposition of Zr on Graphite in Molten Fluorides. *J. Fluorine Chem.* **2011**, *132*, 1122−1126.

(4) Thonstad, J.; Fellner, P.; Haarberg, G. M.; Hives, J.; Kvande, H.; Sterten, Å. *Aluminium Electrolysis: Fundamentals of the Hall-Héroult Process*; Düsseldorf: Aluminium-Verlag, 2001.

(5) Lacassagne, V.; Bessada, C.; Florian, P.; Bouvet, S.; Ollivier, B.; Coutures, J. P.; Massiot, D. Structure of High-Temperature NaF−AlF_3−Al_2O_3 Melts: A Multinuclear NMR Study. *J. Phys. Chem. B* **2002**, *106*, 1862−1868.

(6) Robert, E.; Lacassagne, V.; Bessada, B.; Massiot, D.; Gilbert, B.; Coutures, J. P. Study of NaF-AlF(3) Melts by High-Temperature Al-27 NMR Spectroscopy: Comparison with Results from Raman Spectroscopy. *Inorg. Chem.* **1999**, *38*, 214−217.

(7) Nuta, I.; Veron, E.; Matzen, G.; Bessada, C. High Temperature NMR Study of Aluminum Metal Influence on Speciation in Molten NaF-AlF(3) Fluorides. *Inorg. Chem.* **2011**, *50*, 3304−3312.

(8) Gilbert, B.; Materne, T. Reinvestigation of Molten Fluoroaluminate Raman Spectra: The Question of the Existence of AlF52− Ions. *Appl. Spectrosc.* **1990**, *44*, 299−305.

(9) Tixhon, E.; Robert, E.; Gilbert, B. The Molten MF-AlF3-MCl System (M = K, Na): A Study by Raman Spectroscopy. *Vib. Spectrosc.* **1996**, *13*, 91−98.

(10) Dewing, E. W. Proceedings of the 5th International Symposium on Molten Salts. *Electrochemical Society Inc.* **1986**, 262.

(11) Solheim, A.; Sterten, Å. Thermodynamic Models for NaF-AlF3Melts. *Tenth Aluminium Symposium* **1999**, 13.

(12) Khramov, A. P.; Shurov, N. I. Modern Views on the Composition of Anionic Oxy-Fluoride Complexes of Aluminium and Their Rearrangement During the Electrolysis of Cryolite-Alumina Melts. *Russ. Metall.* **2014**, *2014*, 581−592.

(13) Liška, M.; Perichta, P.; Nagy, L. T. The Structure of MD Simulated Cryolite Melt. *J. Non-Cryst. Solids* **1995**, *192−193*, 309−311.

(14) Akdeniz, Z.; Madden, P. A. Raman Spectra of Ionic Liquids: A Simulation Study of AlF3 and Its Mixtures with NaF. *J. Phys. Chem. B* **2006**, *110*, 6683−6691.

(15) Cikit, S.; Akdeniz, Z.; Madden, P. A. Structure and Raman Spectra in Cryolitic Melts: Simulations with an ab Initio Interaction Potential. *J. Phys. Chem. B* **2014**, *118*, 1064−1070.

(16) Castiglione, M. J.; Ribeiro, M. C. C.; Wilson, M.; Madden, P. A. Al^{3+} Coordination in Cryolitic Melts: A Computer Simulation Study. *Z. Naturforsch., A: Phys. Sci.* **1999**, *54*, 605−610.

(17) Foy, L.; Madden, P. A. Ionic Motion in Crystalline Cryolite. *J. Phys. Chem. B* **2006**, *110*, 15302−15311.

(18) Pauvert, O.; Zanghi, D.; Salanne, M.; Simon, C.; Rakhmatullin, A.; Matsuure, H.; Okamoto, Y.; Vivet, F.; Bessada, C. In Situ Experimental Evidence for a Nonmonotonous Structural Evolution with Composition in the Molten LiF-ZrF4 System. *J. Phys. Chem. B* **2010**, *114*, 6472−6479.

(19) Gheribi, A. E.; Salanne, M.; Chartrand, P. Formulation of Temperature-Dependent Thermal Conductivity of NaF, *β*-Na3AlF6, Na5Al3F14, and Molten Na3AlF6 Supported by Equilibrium Molecular Dynamics and Density Functional Theory. *J. Phys. Chem. C* **2016**, *120*, 22873−22886.

(20) Bučko, T.; Šimko, F. On the Structure of Crystalline and Molten Cryolite: Insights From the ab initio Molecular Dynamics in NpT Ensemble. *J. Chem. Phys.* **2016**, *144*, 064502.

(21) Salanne, M.; Rotenberg, B.; Jahn, S.; Vuilleumier, R.; Simon, C.; Madden, P. A. Including Many-body Effects in Models for Ionic Liquids. *Theor. Chem. Acc.* **2012**, *131*, 1−16.

(22) Aguado, A.; Madden, P. A. Oxide Potentials from ab initio Molecular Dynamics: An Assessment of Their Transferability. *J. Chem. Phys.* **2003**, *118*, 5718−5728.

(23) Ercolessi, F.; Adams, J. B. Interatomic Potentials from First-Principles Calculations: The Force-Matching Method. *EPL Europhys. Lett.* **1994**, *26*, 583−588.

(24) Clark, S. J.; Segall, M. D.; Pickard, C. J.; Hasnip, P. J.; Probert, M. I. J.; Refson, K.; Payne, M. C. First Principles Methods Using CASTEP. *Z. Kristallogr. - Cryst. Mater.* **2005**, *220*, 567−570.

(25) Segall, M. D.; Lindan, P. J. D.; Probert, M. J.; Pickard, C. J.; Hasnips, P. J.; Clark, S. J.; Payne, M. C. First-principles Simulation: Ideas, Illustrations and the CASTEP Code. *J. Phys.: Condens. Matter* **2002**, *14*, 2717−2744.

(26) Rollet, A.-L.; Sarou-Kanian, V.; Bessada, C. Self-diffusion Coefficient Measurements at High Temperature by PFG NMR. *C. R. Chim.* **2010**, *13*, 399−404.

(27) Bonafous, L.; Ollivier, B.; Auger, Y.; Chaudret, H.; Bessada, C.; Massiot, D.; Coutures, J. P. *J. Chim Phys. Biol.* **1995**, *92*, 1867−1870.

(28) Lacassagne, V.; Bessada, C.; Ollivier, B.; Massiot, D.; Florian, P.; Coutures, J. P. Al-27, Na-23, F-19 NMR Study of Cryolite at the

Solid/Liquid Transition. *C. R. Acad. Sci., Ser. IIb: Mec., Phys., Chim., Astron.* **1997**, *325*, 91−98.
(29) Sarou-Kanian, V.; Rollet, A.-L.; Salanne, M.; Simon, C.; Bessada, C.; Madden, P. A. Diffusion Coefficients and Local Structure in Basic Molten Fluorides: in situ NMR Measurements and Molecular Dynamics Simulations. *Phys. Chem. Chem. Phys.* **2009**, *11*, 11501−11506.
(30) Born, M.; Huang, K. *Dynamical Theory of Crystal Lattices*; Oxford University Press, 1954.
(31) Salanne, M.; Madden, P. A. Polarization Effects in Ionic Solids and Melts. *Mol. Phys.* **2011**, *109*, 2299−2315.
(32) Perdew, J. P.; Burke, K.; Ernzerhof, M. Generalized Gradient Approximation Made Simple. *Phys. Rev. Lett.* **1996**, *77*, 3865−3868.
(33) Kresse, G.; Hafner, J. Ab initio Molecular-Dynamics Simulation of the Liquid-Metal-Amorphous-Semiconductor Transition in Germanium. *Phys. Rev. B: Condens. Matter Mater. Phys.* **1994**, *49*, 14251−14269.
(34) Kresse, G.; Hafner, J. Ab initio Molecular Dynamics for Liquid Metals. *Phys. Rev. B: Condens. Matter Mater. Phys.* **1993**, *47*, 558−561.
(35) Kresse, G.; Furthmüller, J. Efficient Iterative Schemes for ab initio Total-Energy Calculations Using a Pane-Wave Basis Set. *Phys. Rev. B: Condens. Matter Mater. Phys.* **1996**, *54*, 11169−11186.
(36) Kresse, G.; Furthmüller, J. Efficiency of ab-initio Total Energy Calculations for Metals and Semiconductors Using a Plane-Wave Basis Set. *Comput. Mater. Sci.* **1996**, *6*, 15−50.
(37) Grimme, S.; Antony, J.; Ehrlich, S.; Krieg, H. A Consistent and Accurate ab initio Parametrization of Density Functional Dispersion Correction (DFT-D) for the 94 Elements H-Pu. *J. Chem. Phys.* **2010**, *132*, 154104.
(38) Mostofi, A. A.; Yates, J. R.; Lee, Y.-S.; Souza, I.; Vanderbilt, D.; Marzari, N. wannier90: A Tool for Obtaining Maximally-Localised Wannier Functions. *Comput. Phys. Commun.* **2008**, *178*, 685.
(39) Marzari, N.; Vanderbilt, D. Maximally Localized Generalized Wannier Functions for Composite Energy Bands. *Phys. Rev. B: Condens. Matter Mater. Phys.* **1997**, *56*, 12847−12865.
(40) Aguado, A.; Bernasconi, L.; Jahn, S.; Madden, P. A. Multipoles and Interaction Potentials in Ionic Materials from Planewave-DFT Calculations. *Faraday Discuss.* **2003**, *124*, 171−184.
(41) Fletcher, R. A New Approach to Variable Metric Algorithms. *Computer Journal* **1970**, *13*, 317−322.
(42) Hutchinson, F.; et al. A Unified Description of MCI 3 Systems with a Polarizable Ion Simulation Model. *Mol. Phys.* **2001**, *99*, 811−824.
(43) Madden, P. A.; Wilson, M. 'Covalent' effects in 'ionic' systems. *Chem. Soc. Rev.* **1996**, *25*, 339−350.
(44) Pauvert, O.; Salanne, M.; Zanghi, D.; Simon, C.; Reguer, S.; Thiaudière, D.; Okamoto, Y.; Matsuura, H.; Bessada, C. Ion Specific Effects on the Structure of Molten AF-ZrF_4 Systems (A(+) = Li+, Na +, and K+). *J. Phys. Chem. B* **2011**, *115*, 9160−9167.
(45) Martyna, G. Constant Pressure Molecular Dynamics Algorithms. *J. Chem. Phys.* **1994**, *101*, 4177.
(46) Martyna, G.; Klein, M. L.; Tuckerman, M. E. Nosé-Hoover Chains: The Canonical Ensemble via Continuous Dynamics. *J. Chem. Phys.* **1992**, *97*, 2635−2643.
(47) Dumez, J.-N.; Pickard, C. J. Calculation of NMR Chemical Shifts in Organic Solids: Accounting for Motional Effects. *J. Chem. Phys.* **2009**, *130*, 104701.
(48) Robinson, M.; Haynes, P. D. Dynamical Effects in ab initio NMR Calculations: Classical Force Fields Fitted to Quantum Forces. *J. Chem. Phys.* **2010**, *133*, 084109.
(49) Pickard, C. J.; Mauri, F. All-electron Magnetic Response with Pseudopotentials: NMR Chemical Shifts. *Phys. Rev. B: Condens. Matter Mater. Phys.* **2001**, *63*, 245101.
(50) Yates, J. R.; Pickard, C. J.; Mauri, F. Calculation of NMR Chemical Shifts for Extended Systems Using Ultrasoft Pseudopotentials. *Phys. Rev. B: Condens. Matter Mater. Phys.* **2007**, *76*, 024401.
(51) Monkhorst, H. J.; Pack, J. D. Special Points for Brillouin-zone Integrations. *Phys. Rev. B* **1976**, *13*, 5188−5192.
(52) Sadoc, A.; Biswal, M.; Body, M.; Legein, C.; Boucher, F.; Massiot, D.; Fayon, F. NMR Parameters in Column 13 Metal Fluoride Compounds (AlF3, GaF3, InF3 and TlF) from first principle Calculations. *Solid State Nucl. Magn. Reson.* **2014**, *59*−*60*, 1−7.
(53) Janz, G. J.; Gardner, G. L.; Krebs, U.; Tomkins, R. P. T. Molten Salts: Volume 4, Part 1, Fluorides and Mixtures Electrical Conductance, Density, Viscosity, and Surface Tension Data. *J. Phys. Chem. Ref. Data* **1974**, *3*, 1.
(54) Corradini, D.; Madden, P. A.; Salanne, M. Coordination Numbers and Physical Properties in Molten Salts and their Mixtures. *Faraday Discuss.* **2016**, *190*, 471−486.
(55) Bale, C. W.; Chartrand, P.; Degterov, S. A.; Erikson, G.; Hack, K.; Mahfoud, R. B.; Melançon, J.; Pelton, A. D.; Petersen, S. FactSage Thermochemical Software and Databases - Recent Developments. *CALPHAD: Comput. Coupling Phase Diagrams Thermochem.* **2009**, *26*, 295−311.
(56) Hu, X.-W.; Wang, Z.-W.; Gao, B.L.; Shi, Z.-n.; Kan, H.-m.; Luo, X.-d.; Tao, W.-j. Equivalent Conductivity and its Activation Energy of NaF-AlF_3 Melts'. *Trans. Nonferrous Met. Soc. China* **2009**, *19*, 719−723.
(57) Yeh, I.-C.; Hummer, G. System-Size Dependence of Diffusion Coefficients and Viscosities from Molecular Dynamics Simulations with Periodic Boundary Conditions. *J. Phys. Chem. B* **2004**, *108*, 15873−15879.
(58) Gobet, M.; Sarou-Kanian, V.; Rollet, A.-L.; Salanne, M.; Simon, C.; Bessada, C. Transport Properties in Cryolitic Melts: NMR Measurements and Molecular Dynamics Calculations of Self-Diffusion Coefficients. *ECS Trans.* **2010**, *33*, 679−684.

DOI: 10.1021/acs.jpcc.7b01530
J. Phys. Chem. C 2017, 121, 10289−10297